JOURNAL OF GEOPHYSICAL RESEARCH, VOL. 106, NO. A12, PAGES 29,669–29,682, DECEMBER 1, 2001

A new particle population near the high-latitude plasma sheet

M. Wilber[1], Q. Li[2], R. M. Winglee, G. K. Parks[1] and M. McCarthy

Geophysics Program, University of Washington, Seattle, Washington

R. P. Lin

Space Sciences Laboratory, University of California, Berkeley, California

Abstract. We present observations of a new, intermediate-energy particle population between the lobe and the plasma sheet. These were seen during two equatorial magnetosphere transits by the Wind spacecraft, when it was 15 R_E distant from the Earth, south of the current sheet and near 0300 local time, and tended to overlap tail-thinning episodes. The observed plasma bulk parameters exhibited a continuous transition from characteristics of the plasma sheet to those of the lobe, suggesting either a mixing region for particles from the two regions, or a transport layer where some processes condition the plasma as it moves from one region to the other. While temperature and density are typically shown to be anticorrelated throughout equatorial transits which span the plasma sheet and the magnetosheath, these two parameters were seen to be positively correlated during the intervals when the new population was observed. Particle distributions obtained by the 3-D Plasma Experiment (3DP) electrostatic analyzers (0.08–27 keV ions; 0.02–28 keV electrons) during these periods often include a kidney-shaped low-energy ion component that appears like the conics commonly seen at low altitudes. These components indicate a likely transverse acceleration mechanism which can extend nearly out to the orbit of Wind.

1. Introduction

One quarter century after they were originally identified, the boundary layers of the magnetosphere remain areas of vigorous study [*Song et al.*, 1995; *Scholer and Treumann*, 1997; *Lundin*, 1997] because the physical processes and the magnetic field topologies associated with them are not well understood. However, an understanding of the magnetopause and its connected boundary layers is critical to any description of mass, momentum and energy transfer between the magnetosheath and the magnetosphere, and hence to our conceptions of the engines powering the dynamic processes observed within the magnetotail. Furthermore, boundary layers couple important magnetopause and tail regions to the ionosphere and are intimately connected to global current and convection systems [e.g., *Lotko and Sonnerup*, 1995].

A majority of magnetopause boundary layer studies have concentrated on the dayside [e.g., *Eastman and Hones*, 1979; *Hall et al.*, 1990; *Song et al.*, 1993; *Paschmann et al.*, 1993; *Fuselier et al.*, 1995; *Phan and Paschmann*, 1996; *Phan et al.*, 1996], although recent publications include results from the Geotail and Wind spacecraft transits on the duskside [*Phan et al.*, 1997; *Fujimoto et al.*, 1998a] and the dawnside [*Fujimoto et al.*, 1998a; *Li et al.*, 2000]. An important observation is that the plasma temperature and density parameters can be strongly anticorrelated, and can exhibit smooth, continuous transitions from the outer low-latitude boundary layer (LLBL) to the central plasma sheet in the face of apparent discontinuities in the time series data. Similar behavior has been seen for electrons in dayside crossings [*Parks et al.*, 1978; *Hapgood and Bryant*, 1990]. This has been interpreted to mean that the boundaries may actually be smooth, with a mixing of low-energy magnetosheath and high-energy magnetosphere plasmas, and that the observed jumps in time series data may result from sudden motions of the boundary layer that are driven by external solar wind conditions.

During the first four years following its launch in late 1994, the Wind spacecraft transited the magnetosphere 26 times along equatorial trajectories. These orbits have been favorable for investigating low-latitude regions of the magnetotail and of the LLBL along the dayside and both flanks up to several R_E tailward of the terminator. To date, we have examined 18 of these orbits in detail, and in this article we present findings of new plasma characteristics that were observed between the plasma sheet and the lobe during two tail passes, when the spacecraft was 15 R_E distant from the Earth and near 0300 local time. In particular, there were extended periods exceeding an hour's duration during which temperature and density parameters were positively correlated and spanned the range between values found in

[1] now at Space Sciences Laboratory, University of California, Berkeley, California

[2] now at Alien Technology, 18410 Butterfield Blvd., Morgan Hill, California

Paper number 2000JA900155.
0148-0227/01/2000JA900155$09.00

the lobe and in the plasma sheet. In addition, for one of these cases, kidney-shaped components were observed in the ion distributions throughout the duration of the event. These components have implications about likely acceleration histories for the associated particles, and may imply that they had a source different from that for other ions seen simultaneously.

We begin in section 2 with a brief description of the Wind instrumentation used in this study, followed in section 3 with observations obtained during three outbound magnetotail passes. The first of these is representative of a "typical" transit, and is provided to establish a baseline for comparison. After summarizing results in section 4, we discuss their likely implications and the questions they raise in section 5.

2. Instrumentation

For this study we have used data obtained from the Wind spacecraft's 3-D Plasma Experiment (3DP) and Magnetic Field Investigation (MFI). The 3DP experiment is a collection of electrostatic analyzers (ESAs) and solid state telescopes (SSTs) designed for studying a wide variety of plasmas that are encountered inside the magnetosphere and the magnetosheath, and in the solar wind. Three SST arrays are used to detect energetic particles (60 keV–7 MeV ions and 26–519 keV electrons), and these obtain 3-D distributions every 3 or 6 seconds. A group of four ESAs record particles of low and intermediate energies, with one pair designed especially for measuring the high phase space density (PSD), cold cores of solar wind ion and electron distributions. All four analyzers have very similar hemispherical designs and sample either 180° or 360° in a plane at any instant, resulting in 4π sr integrations either once or twice per 3-s spacecraft spin period. The high-sensitivity ion and low-sensitivity electron analyzers, PESA High and EESA Low, respectively, have total geometry factors of $\sim 1.5 \times 10^{-2} E\,\mathrm{cm^2 sr}$, with E the analyzer acceptance energy. The high sensitivity electron analyzer, EESA High, is physically larger than the others, yielding a very high geometry factor of $\sim 10^{-1} E\,\mathrm{cm^2 sr}$. The low sensitivity ion analyzer, PESA Low, has an attenuating grid with a resulting geometry factor of $\sim 1.5 \times 10^{-4} E\,\mathrm{cm^2 sr}$.

The EESA Low and EESA High analyzers record electrons in the overlapping energy ranges of 8 eV to 1.1 keV and 80 eV to 27 keV, respectively. PESA High records ions in the energy per charge range of 80 eV q^{-1} to 27 keV q^{-1}. Generally, a full 3-D distribution is obtained onboard Wind each 3-s spin period, but because of telemetry constraints, only selected data are returned to Earth. Depending upon the operating mode, ion distributions are typically integrated over 8–16 spin periods before being telemetered; and single-spin electron distributions are sent once every 8–32 spacecraft rotations. More details about the Wind/3DP investigation can be found in the work of *Lin et al.* [1995]. We have found that for this study, PESA High and EESA Low are the most useful particle detectors, and we will therefore concentrate on data from these instruments.

The MFI experiment includes two tri-axial fluxgate magnetometers which can provide three-component magnetic field vectors. We use averages over 3 s, a time resolution concordant with the shortest particle integrations and comparable to the ion gyroperiod in the plasma sheet. Additional details about MFI are given by *Lepping et al.* [1995].

3. Observations

We have examined the 18 Wind perigee passes from the beginning of Wind's service in November 1994 until the end of 1996. These transits all had equatorial orbits with apogees in the tail, which after the start of 1995 were between 10 and 20 R_E distant from the Earth. The typical near-Earth plasma regions, such as the solar wind, magnetosheath, low-latitude boundary layer, plasma sheet, and lobe, are easily identified by the inspection of plasma parameters and the magnetic field. There were two passes in 1996, March 28 and April 18–19, during which Wind encountered plasma regions not seen during the other equatorial passes we reviewed. Observations of these plasmas persisted for > 1 hour, were associated with tail thinning periods, and occurred while the spacecraft was located a few R_E south of the equatorial plane on the dawnside.

3.1. May 10, 1996

In order to establish a framework within which the new plasma observations can be examined, we begin with observations obtained during the last 8 hours of an equatorial magnetosphere crossing on May 10, 1996. Figure 1 displays plasma parameters computed from ion counts obtained by the 3DP/PESA High detector. The top and bottom panels show density n and temperature T respectively, as estimated from moments of measured distribution functions.

Li et al. [2000] described in detail this outbound magnetosphere transit, which we summarize here. Using particle distributions, they identified five distinct regions: the plasma sheet (labeled "PS" in Figure 1), the cold dense plasma sheet ("CDPS") [cf. *Fujimoto et al.*, 1998b], the low-latitude boundary layer ("LLBL"), the magnetosheath ("MS"), and a layer which they referred to as the magnetosheath boundary layer. [cf. *Fuselier et al.*, 1995, 1997]. We made the classi-

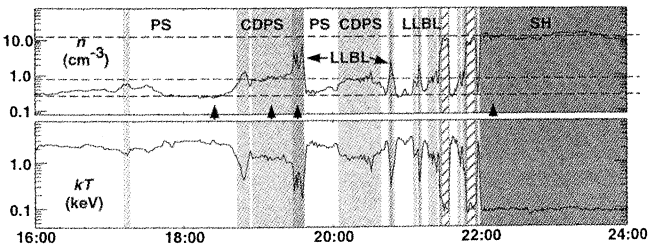

Figure 1. May 10, 1996 PESA High plasma data. (top) Density. (bottom) Temperature. Dark shaded regions following 1934 UT denote the magnetosheath (SH), lightly shaded regions following 1840 UT indicate the low-latitude boundary layer (LLBL), and the medium-dark region prior to 1838 UT marks the plasma sheet. The plasma sheet (PS) and two cold dense plasma sheet (CDPS) regions are also indicated. Upward arrows below top panel indicate intervals for distributions shown in Figures 2 and 3.

fications denoted in Figure 1 using criteria much like those used by *Li et al.* [2000], although we will not distinguish between the magnetosheath boundary layer and the magnetosheath proper in this summary. Regions in this figure are denoted, using successively darker shades, as the plasma sheet (white), the cold dense plasma sheet, the LLBL, and the magnetosheath (darkest). The cross-hatched regions denote the magnetosheath boundary layer. Horizontal dashed lines in the density panel indicate nominal values for the magnetosheath (top), CDPS, and plasma sheet (bottom) .

Figure 2 shows representative ion distributions from each of the four main regions, obtained by the Wind/3DP PESA High ion electrostatic analyzer. The times for these are indicated by the short upward arrows in Figure 1. Distributions

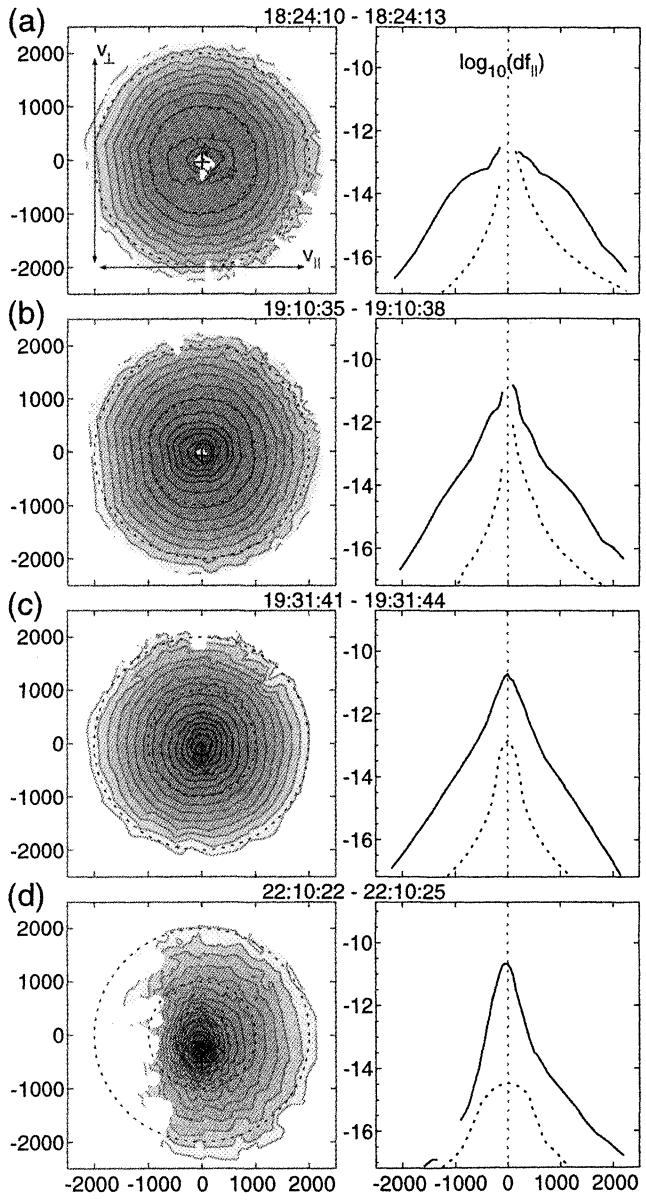

Figure 2. Ion distribution functions (80 eV to 27 keV) for May 10, 1996. Isocontours of particle phase space density in 2-D ($v_{\|}$, $v_{\perp}$) and corresponding 1-D cuts, with dashed lines showing one-count levels. (a) Plasma sheet, (b) CDPS, (c) LLBL, and (d) magnetosheath.

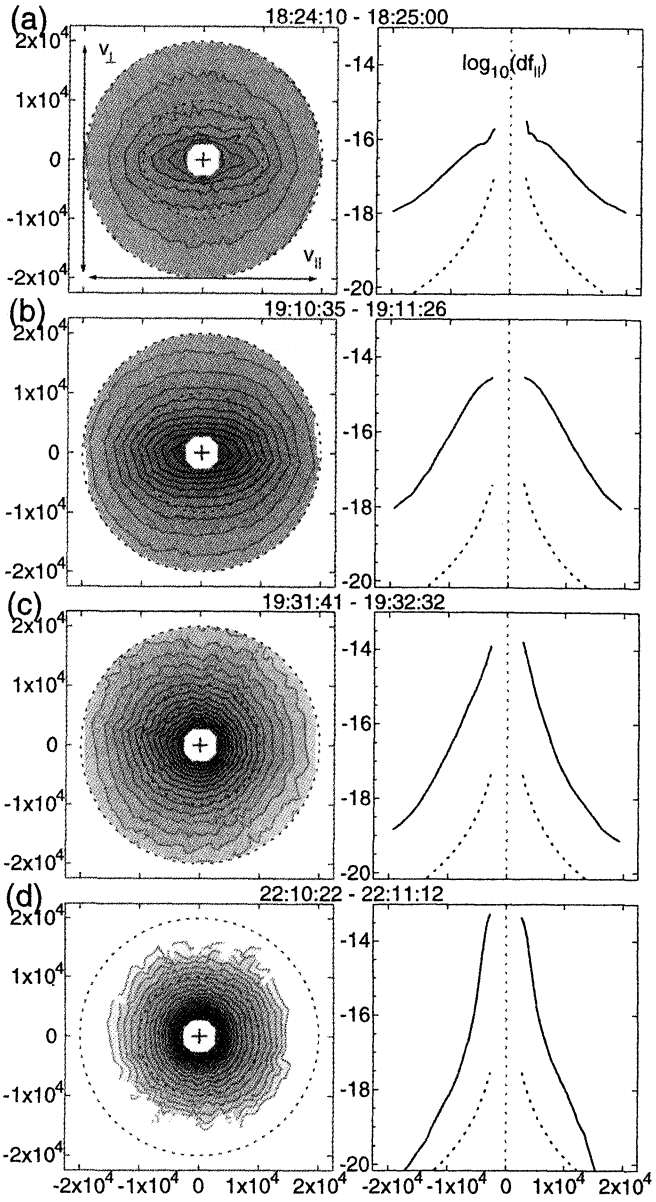

Figure 3. Electron distribution functions (17 eV to 1.1 keV) for May 10, 1996, in the same format as that for Figure 2.

shown here are in the convection frame (i.e., with the perpendicular bulk velocity $\mathbf{u}_{\perp}$subtracted). This has the advantage of showing phase space densities in a frame for which gyrocentric particles are symmetrically distributed about the $u_{\|}$ axis. At the same time, it also retains field-aligned motions ($\mathbf{u}_{\|}$ is not subtracted), so that it is evident which way along the field and at what speed any beams or flows are directed.

The left column shows logarithmically spaced isocontours of ion phase space density in two dimensions ($v_{\|}$, $v_{\perp}$) from PESA High (80 eV to 27 keV q^{-1}) integrated over 51 s. The $v_{\perp}$ values for particles of all gyrophases are rotated onto the vertical axis. (Negative $v_{\perp}$ points correspond to ions with velocities having $\mathbf{v}_{\perp} \cdot \mathbf{u}_{\perp} < 0$; where $\mathbf{u}_{\perp}$ is the component of the bulk flow velocity perpendicular to $\mathbf{B}$.) The right column provides corresponding 1-D cuts along the $v_{\|}$ direction,

with the dotted lines showing one-count levels. Asymmetries in the one-count levels result from the varying angular bin resolutions which are greatest (lowest) in the tailward (sunward) particle directions.

Figures 2a–2d correspond to plasma sheet, CDPS, LLBL, and magnetosheath plasmas, respectively. In the plasma sheet the ions have hot (~2 keV), isotropic distributions, which level off between ~400 and ~1000 km/s. In the cold dense plasma sheet, densities are 2–3 times greater, with ion distributions that are somewhat cooler and which lack the shelf feature from 400 to 1000 km/s. We see that in the LLBL (Figure 2c) the ions have isotropic distributions, with densities and temperatures intermediate between those of the magnetosheath and the CDPS. In the magnetosheath, Wind observed cold ion distributions as expected, with a perpendicular temperature anisotropy that is most prominent in the lower energies, and with a strong asymmetry between field-aligned and anti-aligned phase space densities.

Figure 3 shows data obtained by EESA Low (17 eV to 1.1 keV electrons) integrated for 3 s, and is in the same format as Figure 2. We have excluded data from the three energy bins below 17 eV, since these are contaminated by photoelectrons. The plasma sheet electrons have $T \simeq 200$ eV, with distributions that are isotropic above ~1 keV and which have a strong parallel temperature anisotropy at lower energies. Compared to the plasma sheet proper, the CDPS electron distributions have anisotropic low-energy ($\lesssim$1 keV) cores with higher phase space densities; but higher-energy components with lower PSDs.

While the (time-ordered) moments presented in Figure 1 suggest that Wind encountered boundaries separating each of the regions described above, inspection of all distributions reveals that the distinction between the plasma sheet and the CDPS plasmas is generally a matter of degree; by selecting distributions out of strict time sequence, it is possible to find a series which shows a smooth variation between the distribution seen starting at 1824:09 UT in the plasma sheet and that seen starting at 1910:35 UT in the CDPS. The fairly abrupt changes observed between plasma sheet and CDPS regions may represent sudden motions past the spacecraft of slowly varying magnetotail regions, rather than the passage of Wind through true discontinuities. Some support for this is provided by Figure 4.

Immediately apparent from inspection of Figure 1 is the anticorrelation between the temperature and the density. In plasmas where perpendicular kinetic pressure, $\Sigma_\gamma n_\gamma k_B T_{\perp\gamma}$, dominates magnetic pressure, $B^2/8\pi$, such anticorrelations between n and T might be expected as pressure balance is maintained [cf. *Baumjohann*, 1998], assuming a locally planar geometry and steady exterior forcing by the solar wind. (Here, γ indexes particle species, k_B is the Boltzmann constant, and B is the magnetic field strength.) In order to demonstrate this anticorrelation explicitly, and to present this as a baseline for comparison of the two events which follow, the logarithms of temperature versus density are shown as a scatterplot in Figure 4. Dark pluses toward the lower right denote the magnetosheath, light pluses in the upper left indicate the plasma sheet, and medium-dark pluses mark the LLBL and the CDPS.

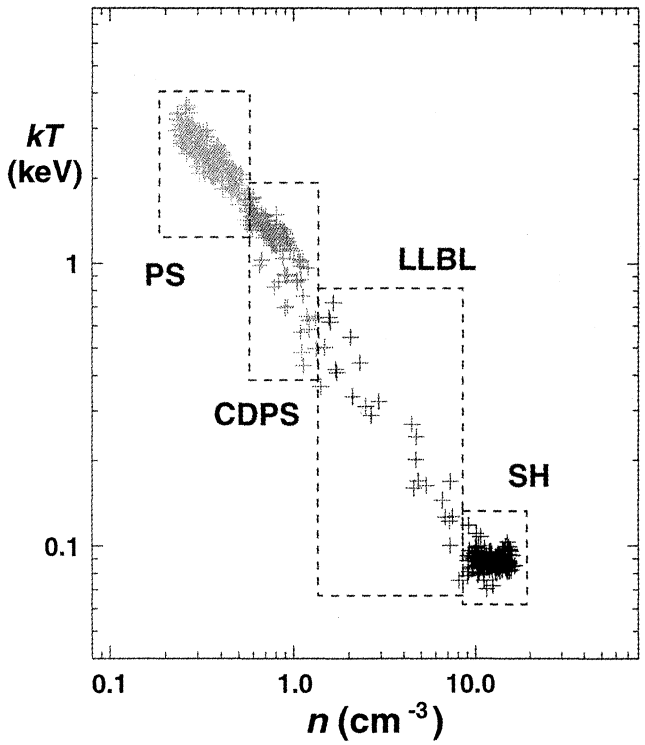

Figure 4. May 10, 1996 $\log(T)$ versus $\log(n)$ correlation. Dark pluses denote the magnetosheath, medium-dark pluses indicate LLBL/CDPS plasma, and light pluses mark the plasma sheet and cold dense plasma sheet.

The nearly continuous spread of points in Figure 4 lends support to the assertion made above that the discontinuous transitions observed between the various plasma regions need not imply sharp physical boundaries, and may in some cases have been the result of rapid motions of the magnetotail due to variations in exterior conditions. [Cf. *Hapgood and Bryant*, 1990; *Hall et al.*, 1990; *Phan et al.*, 1997, .]

3.2. March 28, 1996

On March 28, 1996 Wind completed the outbound portion of the earliest perigee pass discussed in this section. Figures 5a–5d present Wind plasma moments, n, v_x, and T, and magnetic field data, for 0100–1300 UT. At 0600 UT, Wind was located at (-7.8, -13.3, -3.6) R_E (GSM), and IMP 8 was in the solar wind at (-4.7, 33.1, 12.5) R_E. IMF data from IMP 8/MAG were available for the first 5.25 hours of this interval, and are shown in Figure 5. The IMF turned dawnward around 0235 UT and southward near 0245 UT, with an estimated propagation time to the magnetosphere of 5 min.

At 0307 UT the spacecraft entered a region where the densities were elevated and the temperatures were often substantially reduced relative to those of the surrounding plasma sheet, and where T and n were roughly correlated. These conditions persisted until 0524 UT. This ~2.25 hour inter-

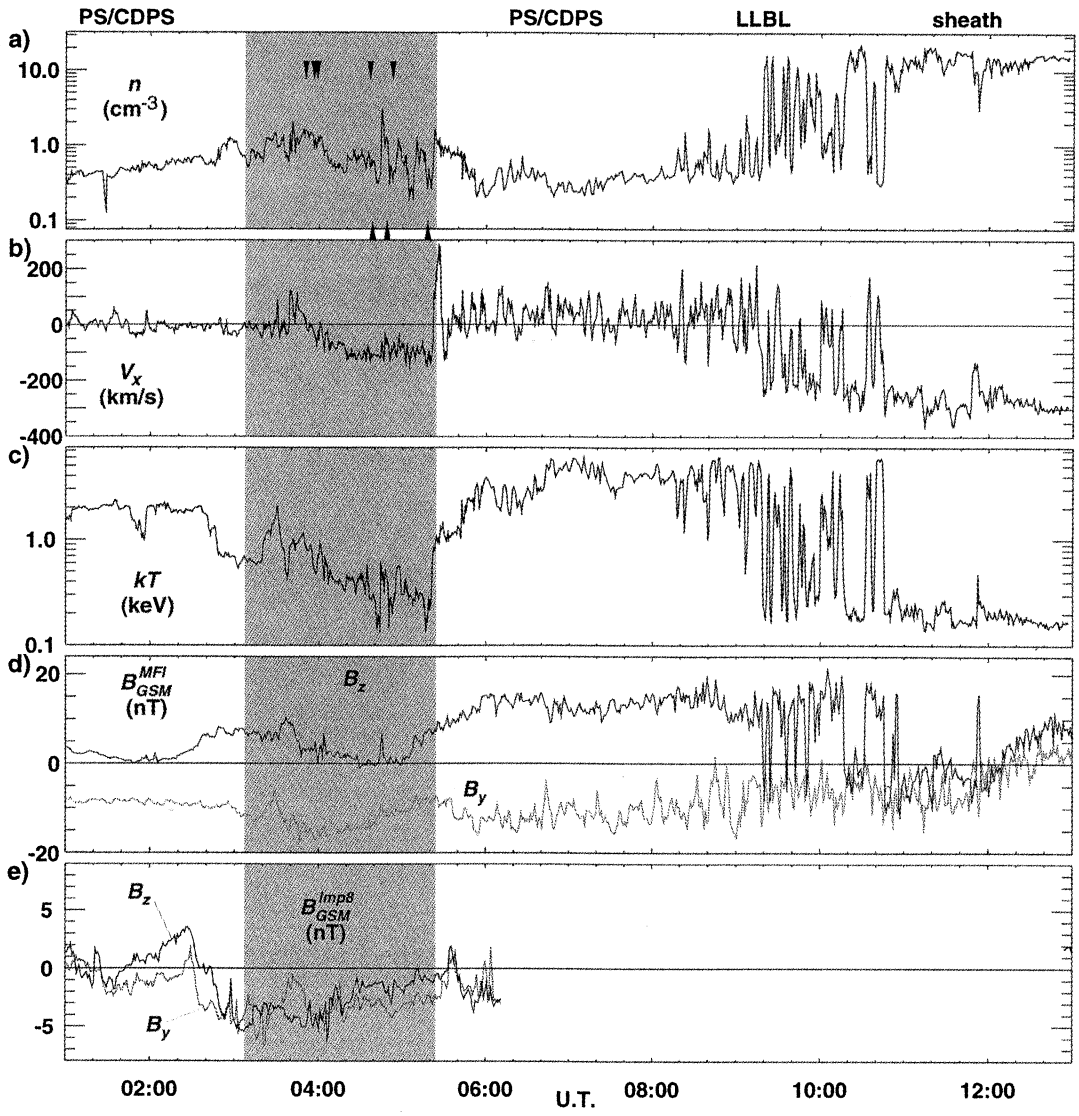

Figure 5. March 28, 1996 bulk parameters. (a) Plasma density, (b) velocity, (c) temperature, (d) GSM magnetic field components, and (e) GSM y and z components of the interplanetary magnetic field (IMF). Downward arrows above the density trace denote intervals plotted in Figures 7 and 8, while upward arrows below the trace correspond to the distributions of Figure 9.

val, shaded in Figure 5, will be the focus of the discussion which follows. During the second half of this interval, the computed velocity moments show values around 100 km/s tailward, following a shorter 15 minute interval of $\lesssim$100 km/s earthward flow. After reentering the plasma sheet, Wind remained there until 0816 UT, at which time it began to sample the low-latitude boundary layer. The spacecraft encountered the magnetopause for the first of several times at 0920 UT, and made its final exit from the magnetosphere into the magnetosheath at 1154 UT. The x component of the magnetic field (not shown) remained tailward between 7 and 40 nT until Wind began to sample the LLBL around 0816 UT, after which time it exhibited large $\delta B/B$ fluctuations.

After Wind reentered the plasma sheet at 0524 UT, the density and temperature values exhibited a strong anticorrelation similar to that observed on May 10, 1996 (Figures 4 and 1). This is shown more clearly in Figure 6, which is a scatterplot of $\log(T)$ versus $\log(n)$. Data from Figure 5 are plotted with black pluses denoting points obtained during the shaded region, and with grey pluses representing points from the plasma sheet, LLBL and magnetosheath. As was the case on May 10, the LLBL forms a continuous link between the magnetosheath and the plasma sheet, suggesting a smooth mixing or diffusion of plasma components.

What is new is the positively correlated branch extending from the lower left of Figure 6 to the center of the LLBL—plasma sheet transition. Although the densities do not reach down to the barely measurable low values often seen in the lobe, the location of the spacecraft and the combination of low values for both density and temperature make the association with the lobe clear. It should be noted that Wind

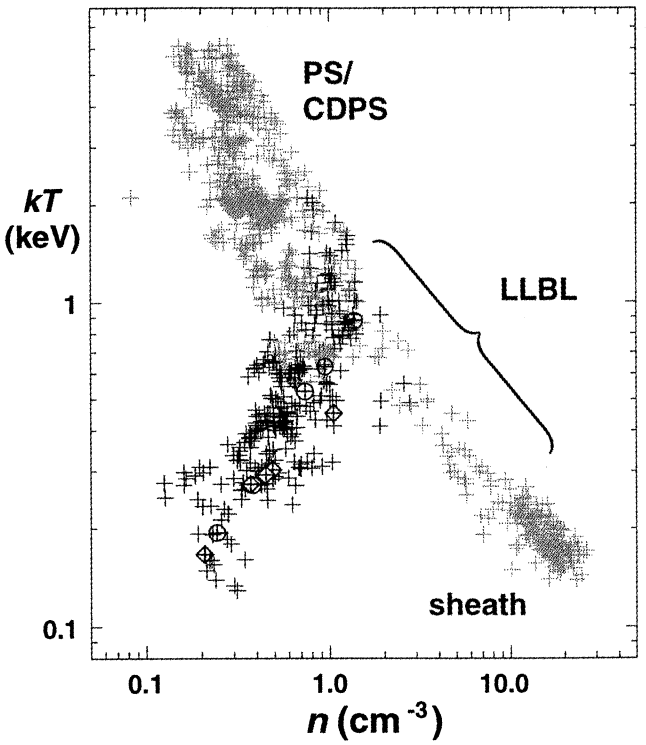

Figure 6. Scatterplot of $\log(T)$ versus $\log(n)$ for March 28, 1996. Here, grey pluses represent observed values from the LLBL, the plasma sheet, and the magnetosheath, while black pluses represent points obtained during 0307–0524 UT. Circled points correspond to the distributions in Figures 7 and 8, while points with diamonds correspond to the distributions shown in Figure 9.

observations of the lobe during other magnetosphere passes (e.g., 0830–0940 UT and 1010–1210 UT, September 17, 1995; 0718–0805 UT, November 29, 1995; 0530—0630 UT, January 13, 1996; 1553–1630 UT, September 9, 1997) show that it typically appears as an anticorrelated branch in $\log(T)$ versus $\log(n)$ scatterplots. Positively correlated branches connecting the LLBL—plasma sheet and lobe branches can sometimes be found, but the cases presented in this paper are the most clear found to date. It is commonly observed that lobe-plasma sheet transitions are nearly discontinuous, indicating a rapidly moving or a physically restricted boundary [*Eastman et al.*, 1985]. The observations composing the positively correlated branch of Figure 6 persisted for 2 hours and 25 min, and therefore are suggestive of a broad region. For this reason, we refer to this as the lobe-plasma sheet transition layer (LPSL).

The continuity of points is also important, as it indicates a smooth transition between plasma in the center of Figure 6 and the lower left edge. In other words, the center of this figure, which corresponds roughly to plasma from the cold dense plasma sheet, appears to be the intersection of material associated with the central plasma sheet (upper left), the magnetosheath (lower right), or the lobe (lower left). In principle, this LPSL could result from particles escaping the plasma sheet into the lobe, or from lobe material merging into the plasma sheet. To decide between these, in the absence of a measurable convection rate in the north-south direction (i.e., below ~20 km/s), we refer to the distribution functions for clues.

Figure 7 shows individual ion distributions at five times sampled during the positively correlated branch of the $\log(T)$ versus $\log(n)$ plot. These are ordered from top to bottom by

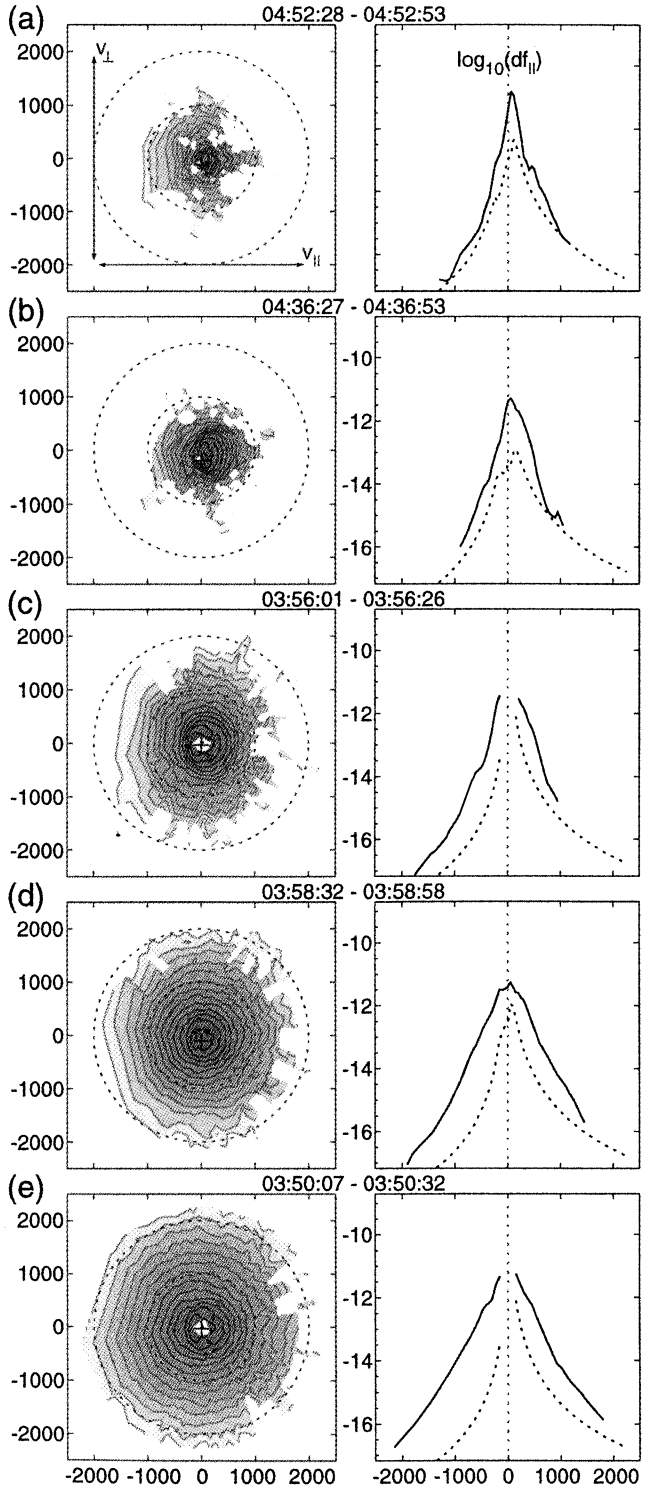

Figure 7. (a–e) Ion distributions (80 eV to 27 keV) for March 28, 1996, in the same format as that for Figure 2.

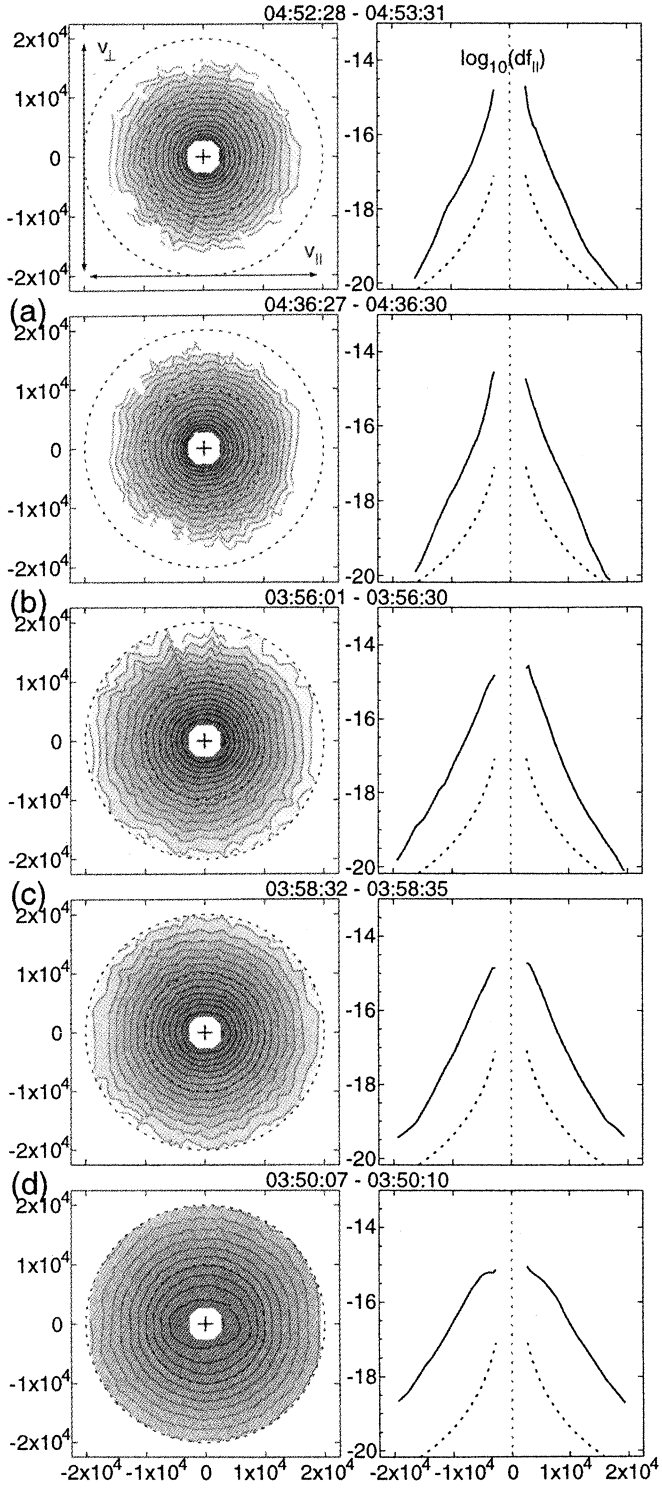

Figure 8. Electron distributions (17 eV to 1.1 keV) for March 28, 1996, in the same format as that for Figure 3.

increasing density and also were computed in the $\mathbf{u}_\perp$ reference frame. The format is the same as that for Figure 2, with isocontours of ion phase space density in 2-D $(v_\parallel, v_\perp)$ space in the left column, and corresponding 1-D cuts in the right column. Corresponding times are shown as downward pointing arrows above the density trace in Figure 5a, and as circled points in Figure 6.

At first glance, these plots merely reproduce what can be inferred from the plasma moments: that the distributions are getting generally wider as the density increases (i.e., as samples progress away from the lobelike region plotted in Figure 7a). Excluding the CDPS distribution (Figure 7e) these have modest perpendicular temperature excess. Some of these, most notably the two beginning at 0436:27 and 0356:01 UT, have distinct low-energy components, which will be discussed in more detail below.

Figure 8 shows EESA Low electron distributions in the same format as that used for Figures 2, 3, and 7. These correspond to times for the ion distributions presented in Figure 7. As was the case for all of the LLBL and plasma sheet electron distributions in Figure 3, the distribution having the highest density and best representing the usual plasma sheet, 0350:07 UT, has a parallel temperature excess at the lowest energies. The lower-density distributions, at 0356:01 UT, e.g., are isotropic for all energies. Processes leading to the bi-streaming core electrons in the LLBL and plasma sheet do not appear to occur within this transition layer. The 1-D cuts for 0356:01 and 0358:32 UT indicate that there is a possible admixture of the bi-streaming component which is lower by two orders of magnitude from that seen at 0350:07 UT while inside the CDPS. The isotropy of the LPSL electrons is also in contrast to the weakly perpendicular ion distributions obtained at the same times.

The presense of low-energy components within ion distributions on 28 March 1996 (e.g., starting at 0436:27 and 0356:01 UT) warranted additonal scrutiny. Upon inspection of other distributions within the LPSL branch seen in Figure 6, we found that many had these low-energy populations, of which a large fraction had a distinctive appearance. Figure 9 shows the low-velocity portions of five PESA High ion distributions from this region. Corresponding times are shown as upward-pointing arrows below the density trace (top panel) of Figure 5, and as points circumscribed by diamonds in Figure 6.

The format for the left column is the same as in earlier figures, except that the velocity range has been reduced to ± 800 km/s on both axes, rather than the ± 2500 km/s range of previous examples, and the limits for the phase space densities have been restricted accordingly (with corresponding changes to the contour levels). The $\mathbf{u}_\perp$ reference frame is used here as well. These distributions are again ordered by increasing density when going down the page, corresponding to a progression from the lobelike region towards the LLBL—plasma sheet branch. (The chosen thresholds for the velocities and phase space densities clip the high-energy part of these distributions, making their relative order within the layer less evident.)

Apparent in all of the panels in Figure 9 are wedge-shaped low-energy components traveling along the magnetic field direction. Such a wedge-shaped component is also present in the 0436:27 UT distribution of Figure 7. At Wind's location south of the magnetic equator this implies tailward motion. These low-energy components are sitting on top of much hotter distributions. Most of these are dimpled on the field-aligned side, resulting in kidney shapes. In addition,

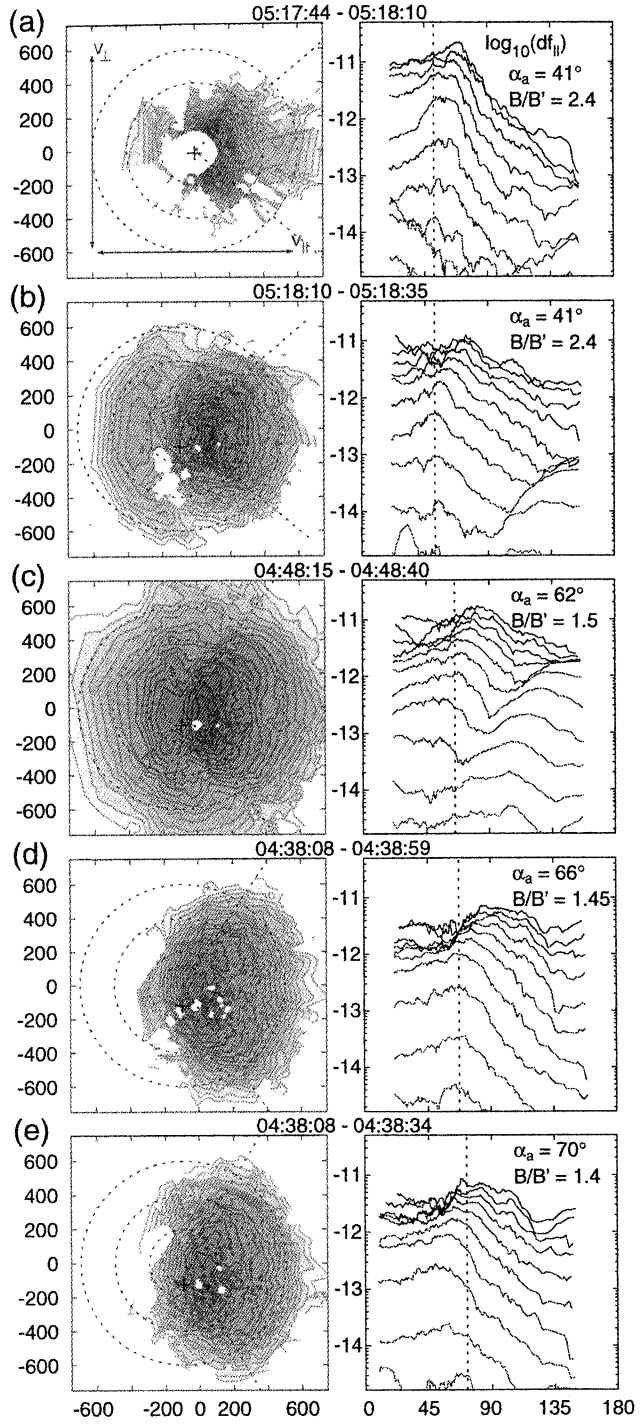

Figure 9. (a–e) Kidney-shaped ion distributions for March 28, 1996, in the same format as that for Figure 2, except that the velocity ranges have been restricted to ±800 km/s and the contouring levels are different. In the right column, phase space densities are plotted as a function of pitch angle, α, for each of the electrostatic analyzer energy bins. The angle α_a and the ratio B/B' are described in the text.

1-D cuts (not shown) reveal that several of these distributions have tailward beams traveling faster than these wedge-shaped components. In several cases, for example, starting at 0448:15 and 0518:10 UT, there are also antifield-aligned beams, which appear to have undergone pitch angle scattering.

The right column of Figure 9 shows corresponding traces of phase space density as a function of pitch angle, α, for the lowest 13 energy channels of the detector. These are used to identify phase space density maxima (marked with dashed vertical lines), which it turns out are neither along the field direction nor perpendicular to it. The pitch angles of these maxima tend to decrease as a function of energy, up to some intermediate energy, and such "asymptotic" values are shown in the left column as dashed diagonal lines.

In other contexts, such kidney-shaped distributions have been associated with ion conics. For the simplest cases, these are explained as originating from beams that have been perpendicularly accelerated, and which subsequently have folded in phase space toward the parallel axis as their constituent particles adiabatically move into weaker magnetic field regions, conserving magnetic moment. It is probable, however, that in most cases the ion conics commonly observed at low altitudes are accelerated over a broad spatial range as they travel along field lines, so that magnetic moments are not conserved [*Whalen et al.*, 1991; *Miyake et al.*, 1993], and it is possible that parallel electric fields might further alter the evolution of the distributions. Nonetheless, for our present purposes we will stick to the simplest scenario, where acceleration occurs in a limited region and particles thereafter travel adiabatically and unperturbed into weaker field regions.

If we assume an original shape for these distributions that was approximately bi-Maxwellian, with $T_\perp/T_\parallel \gg 1$, where for all particles the parallel speeds are essentially the same as the beam speed, it is possible to estimate the magnitude of the magnetic field at the "source" location (i.e., where these were last subjected to perpendicular acceleration). Providing that particle magnetic moments and kinetic energy are conserved as they travel to the observation point, the ratio of the original to the observed field strength is

$$\frac{B}{B'} = \frac{v_\perp'^2 + v_\parallel'^2 - v_\parallel^2}{v_\perp'^2} \tag{1}$$

Here, primes denote observed values, and no primes indicate source values, with $v_\parallel$ and $v_\perp$ a particle's parallel and perpendicular velocities, respectively. Equation (1) describes a hyperbola with asymptotes that have slopes of $s = \pm\sqrt{B'/(B-B')}$, so that $B/B' = 1 + 1/s^2$. These ratios and the asymptotic pitch angles, α_a, are indicated in the right column of Figure 9. The narrowest of these cones, starting at 0517:44 and 0518:10 UT, have half-angles of ~40°, yielding estimated field strengths at the "source" that are 2.4× the observed magnetic fields of ≲40 nT. Using the T96 magnetic field model [*Tsyganenko*, 1989; *Tsyganenko and Stern*, 1996], we have traced a field line threading Wind's position at the time of these observations to points where the fields are increased by this factor of 2.4, and this puts the 'source' region at greater than 10 R_E from the Earth. The widest of these cones, beginning at 0438:08 UT, has a half-angle of ~59°, implying a source field strength of just 1.36 times the observed value, which would place the

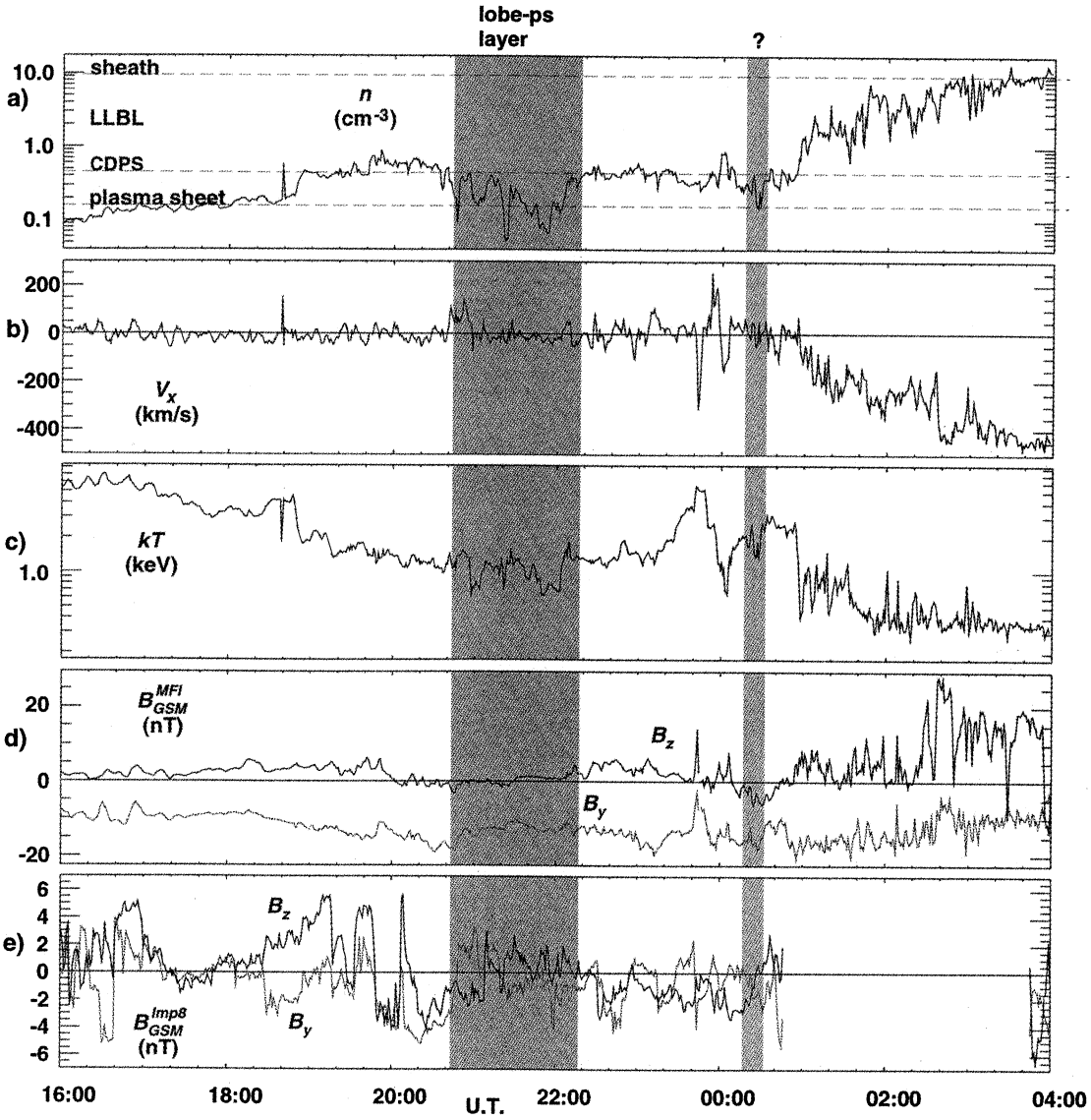

Figure 10. Bulk characteristics of plasma on April 18–19, 1996. (a) Density, (b) tailward velocity, (c) temperature, and (d) magnetic field measured onboard Wind. Shading deliniates different regions labeled at the top, and described more fully in the text.

source much closer to Wind's location 15 R_E from the Earth. Recognizably "conic-like" distributions can be seen to have asymptotes near 70°, implying a source field strength just 10–15% greater than that at the observation point. It is notable that these conic-like distributions are seen throughout the lobe-plasma sheet transition layer.

3.3. April 18–19, 1996

The data for this case were obtained during the last 8 hours of April 18 and the first 4 hours of April 19, 1996. Wind was outbound from the plasma sheet by 1600 UT on April 18 and encountered the low-latitude boundary layer around 0030 UT on April 19. At 0240 UT it crossed the magnetopause for the last time. At 2200 UT on 18 April Wind was located at (-10.8, -11.0, -5.1) R_E (GSM), and IMP 8, again located in the solar wind, was at (32.7, -6.4, 21.1) R_E.

Figure 10 shows plasma parameters and magnetic field values in the same format as that for Figure 5. Dark shading prior to 2000 UT marks the plasma sheet ("PS"); medium-dark shading between 2042 and 2217 UT denotes a region which later will be identified as a lobe-plasma sheet transition layer ("LPSL"); medium-dark sections following 0036 UT correspond to the low-latitude boundary layer ("LLBL"); and the darkest shading on the right side of this figure marks the magnetosheath ("sheath"). A lightly shaded box from 0017 UT to 0032 UT delimits a brief interval that may also be associated with a lobe-plasma sheet transition layer.

The y and z components of the IMF changed several times during this interval. Of interest here is the mainly northward interval starting at 1749 UT and lasting for 2 hours, followed by a mostly southward interval lasting from

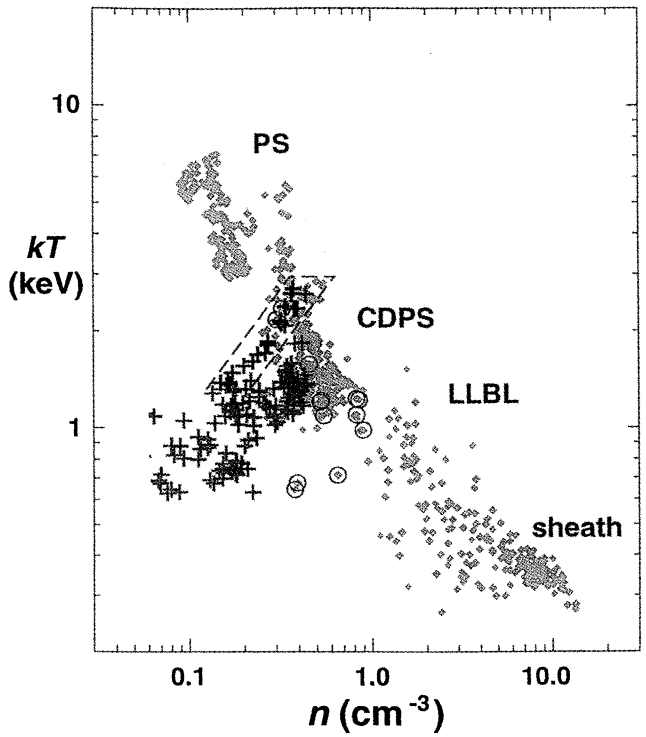

Figure 11. Scatterplot of $\log(T)$ versus $\log(n)$ correlation for April 18–19, 1996. Circled points correspond to intervals showing kidney-shaped components in ion distribution functions near 0000 UT.

1949 until 2107 UT. This southward period was split by a 6 min northward interval starting at 2007 UT. From 1949–2107 UT, the y component of the IMF pointed almost exclusively in the dawnward direction. The x component of the IMF (not shown) was primarily in the sunward direction. The propagation time from IMP 8 to the magnetosphere was ~10 min. Even accounting for this lag, however, the shaded region of interest in Figure 10 trailed the southward turning by ~50 min.

Figure 11 is a scatterplot of $\log(T)$ versus $\log(n)$, which shows that the temperature and density in the plasma sheet and LLBL were anticorrelated as usual and that there was a region inside of which these parameters were positively correlated, as was the case for March 28. Here, the dark pluses identify the positively correlated T versus n regions in Figure 10. In this case there apparently was a second lobe-plasma sheet transition layer, that in Figure 11 is outlined by a narrow, dashed parallelogram and which corresponds to the brief shaded interval between 0017 and 0032 UT in Figure 5.

During this perigee pass no conic-like distributions were seen during the positively correlated T versus n intervals. At times, counterstreaming and isolated earthward ion beams typical of the plasma sheet boundary layer [*Parks et al.*, 1984; *Takahashi and Hones*, 1988] were present. Conic-like distributions were seen, however, during a 10-min interval centered about midnight, which coincided with the passage of Wind through a relatively dense plasma sheet or CDPS region. In Figure 11 these intervals are indicated by circled points. These observations preceded by 10–15 min the second, much briefer LPSL-like transition described above, which was followed by entry into the LLBL.

4. Summary of Observations

We began with a review of a "typical" LLBL—plasma sheet crossing on May 10, 1996, for which we demonstrated the strong anticorrelation that can exist between T and n (Figure 4). We presented "representative" ion (80 eV to 27 keV) and electron (80eV to 1.1 keV) distribution functions (Figures 2 and 3) for the plasma sheet, cold dense plasma sheet (CDPS), low-latitude boundary layer (LLBL) and the magnetosheath. While time series data showed discontinuous jumps and plateaus in the n and T values (Figure 1), the scatterplots showed continuous, quasi-monotonic variations.

Anticorrelations between T and n were also observed on April 18–19 and March 28 for most times (Figures 6 and 11), but there were also branches in these scatterplots which extended from the lower left, with temperatures and densities approaching those seen in the lobe, to the middle of the LLBL—plasma sheet transition. These branches, which we call the lobe-plasma sheet transition layer (LPSL), have not been reported before. The points where the two branches merge correspond to either the LLBL or the CDPS. Within the LLBL—plasma sheet transition it is possible to find particle distributions which conform to those representative samples presented for the plasma sheet, CDPS, LLBL, and magnetosheath of May 10, 1996. The distributions from the LPSL, however, do not resemble those from any of these regions. The lobe observed by Wind typically shows $\log(T)$ to be anticorrelated with $\log(n)$.

Ion distributions obtained within the LPSL on March 28, 1996 often showed kidney-shaped low-energy components, which had phase space density peaks at pitch angles different from 0° and 90°. Pitch angles for these maxima were seen to range from ~40° to near 70°, although for pitch angles approaching 90° such distributions become indistinguishable from those with simple perpendicular temperature anisotropies. Kidney-shaped components were not apparent within the LPSL on April 18–19, but instead were seen while Wind was in the LLBL or possibly in the CDPS. While often absent entirely, isolated ion beams and counterstreaming beams typical of the plasma sheet boundary layer were seen more frequently on this date than on March 28.

5. Discussion

The observations from May 10, 1996 are optimal for illustrating the strong anticorrelation between n and T during LLBL—plasma sheet transits through the magnetotail. The steps and plateaus in the time series data, which are in no way evident in the scatterplot of Figure 4, show how a spacecraft could appear to cross relatively sharp boundaries although the transitions may actually be due in large part to rapid, large-scale motions of the tail.

A number of arguments regarding the positively correlated branches seen in the $\log(T)$ versus $\log(n)$ scatterplots

for April 18 and March 28, 1996 point to an interpretation of these as a new plasma layer, rather than as merely due to temporal changes or as extended observations of the plasma sheet boundary layer. The continuity of the points spanning the new branches in Figures 6 and 11, as well as the continuity of the distribution functions themselves, suggests that this is a smoothly varying, thick layer that extends from the plasma sheet (nearly) to the lobe. The layer cannot by most definitions be considered an unusually thick plasma sheet boundary layer, as the distribution functions sampled within it typically fail to include the quasi-monoenergetic field-aligned beams that characterize those layers. (Compare the distribution functions of Figures 7 and 9 to those presented by *Eastman et al.* [1984, Figure 8] and *Parks et al.* [1998, Figure 2].)

Another possible explanation for the positively correlated branch in Figures 6 and 11 is that Wind was actually sampling the plasma mantle. On March 28, 1996 this interval occurred during a period of southward IMF, when flux transport to the nightside and/or tail thinning might have led to mantle field lines which were sufficiently far equatorward that they could be seen during this nearly equatorial tail crossing. For part of this period the plasma had a bulk velocity near 100 km/s tailward (compare the velocity moments in Figure 5), which would be consistent with expected mantle flows. We do not favor this interpretation for three reasons. First, the flows seen during the early part of the March 28 interval are earthward rather than tailward, and those seen on April 18–19 are near zero, showing that there is no consistent association with tailward plasma motion. Second, rather than increasing in density to levels approaching those of the magnetosheath, the observed plasma densities remained below ~ 1 cm^{-3} (March 28, 1996) or decreased significantly from the values seen in the plasma sheet (April 18–19 1996). Density decreases from values of the plasma sheet would be expected for motion into the lobe, rather than for motions from the lobe or plasma sheet into the mantle. Finally, for the observed layer to be the mantle, the lobe would necessarily have vanished or have been traversed by the spacecraft in a time comparable to the 25–50 second integration period of the 3DP instruments.

The durations of these layers, extending for well beyond 2 hours in the case of March 28, is far longer than is typical for plasma sheet boundary layer transitions [*Eastman et al.*, 1984]. It also seems unlikely that what is being observed is the plasma sheet depopulated of its medium and high-energy particles, since the consequences of losses over such long periods would likely have globally observable effects, which have not been reported. The short-term temporal variations in the moments for March 28, 1996 (Figure 5) seen at ~0240 and ~0520 UT and the much slower variations seen during much of the intervening interval, would seem to require a process or processes which could depopulate and repopulate the region on widely varying timescales. A simpler explanation is that the spacecraft passed through a layer which varies monotonically, and that abrupt motions of the magnetotail at the two endpoints led to discontinuous jumps in plasma parameters; reconfigurations of the magnetotail on convection time scales, as well as sudden motions, are known to occur regularly. We have found that there is a clear correspondence between the observed density fluctuations and the plasma velocities along the z direction (not shown).

In section 3.1 we suggested that the anticorrelations between n and T might be expected as pressure balance is maintained when perpendicular kinetic pressure dominates magnetic pressure. This description clearly does not apply when n and T are positively correlated during observations of the LPSL on April 18 and March 28, 1996. In both of these cases the LPSL was coincident with monotonic total pressure rises (not shown) of the order of 40%, followed by declines to near-original values. While there was a strong anticorrelation between magnetic and kinetic contributions to this, the magnetic pressure component usually dominated and determined the rise and fall of the total. On April 18 the total pressure maximum was coincident with the start of the LPSL observations, while on March 28 the maximum was reached midway through the layer. On April 18, the elevated magnetic pressure interval corresponded closely with the strong tail thinning observed between 2000 and 2200 UT, while on March 28 the tail thinning lagged the pressure maximum by ~40 min. These observations suggest that the LPSL coincided with magnetic flux enhancements in the tail, but the correspondence between the southward turning of the IMF observed by IMP 8, the tail thinning, and the magnetic pressure maximum is not exact.

In some cases the continuity of points seen in plots such as Figure 4 has been taken as partial evidence for diffusion-like processes occuring across the equatorial magnetotail, particularly during northward IMF conditions [*Eastman et al.*, 1976; *Fujimoto et al.*, 1998a, b; *Phan et al.*, 1997]. However, it is a challenging task to establish this unequivocably from single-point measurements of moments alone; diffusion problems are inherently time-dependent, and the intervals over which plasma profiles are measured may be comparable with diffusion timescales. In principle, inspection of distribution functions can be used to discern between populations arising from diffusive processes and simple mixtures created when particles from distinct regions have gained access to a single field line. In the diffusive case, scattering processes would relax contributing components to create a distribution which approached a single Maxwellian with intermediate properties, while in the case of simple mixing, the resulting distributions would appear as linear combinations of the source populations.

Plasma sheet, LLBL, magnetosheath, and (arguably) CDPS distributions similar to the representative ion and electron samples presented for May 10, 1996 (Figures 2 and 3) were seen on April 18 and May 28, 1996 as well. Perhaps most relevent in these is the presence of bistreaming, low-energy ($\lesssim$ 1 keV) electron cores which are most prominent in the CDPS, but which are also present in the plasma sheet. *Li et al.* [2000] used May 10, 1996 Wind observations to argue that these core populations originated near the LLBL, with a fraction persisting in central plasma sheet distributions which was in inverse proportion to the distance from

that boundary layer. These bistreaming electron cores are only minimally present in the LPSL, where they are reduced by 2 orders of magnitude or more, if they can be discerned at all. Their absence argues against an interpretation of the LPSL as a simple mixing layer; if lobe and plasma sheet (or CDPS) particles are mixed within this layer, the low-energy electron component is necessarily being isotropized in the process. This could be accomplished, however, by waves which are commonly observed in the plasma sheet boundary layer [*Parks et al.*, 1984].

On March 28, 1996 there was a clear association between the conic-like distributions (Figure 9) and the LPSL; virtually all of these distributions occurred during that transition interval. Conversely, most distributions within this interval appeared to have had at least some indication of a cold component which could be interpreted as a conic in some stage of continued perpendicular heating or free expansion into weaker field regions. These kidney-shaped distributions may have been observed by ISEE 1 [*Sharp et al.*, 1981; *Horwitz et al.*, 1982], but our main point here is that they have been seen within the LPSL, which has not been identified previously.

Assuming simple adiabatic propagation to account for the kidney-shaped components, we determined the locations of "source regions" using (1) and the T96 magnetic field model. These ions were presumed to have last experienced perpendicular acceleration at the source, after which time their distributions transformed during free expansion into lower field regions. The minimum computed distances from the Earth, corresponding to the narrowest of the kidney-shaped distributions at ~0518 UT, were in excess of 10 R_E, and those with larger asymptotic pitch angles implied sources much closer to the spacecraft. When comparing the T96 model with the observed magnetic fields, we found that the their magnitudes were within ~10% of the measured values, but their directions were not as accurate and did not show the strong tail thinning observed by Wind. However, the magnitudes are what is relevent for the application of (1), and the "source" distances derived therefrom are likely to be provided more accurately due to less perturbation of the magnetic fields closer to the Earth.

On April 18–19, none of the kidney-shaped distribution components was seen within the transition interval. Those which were seen occurred during a 10-min period around midnight (universal time), and were most often on the anticorrelated branch of the T versus n scatterplot. These differences between the times of observed "conic-like" distributions show that, regardless of their source, they apparently can have access to both the LPSL and the LLBL/CDPS.

The positively correlated branches in the T versus n plots for April 18–19 and March 28 had other important differences, which may be related; in the latter case there was a stronger temperature dependence upon density (i.e., a steeper slope), and the LPSL intersected the LLBL—plasma sheet branch at higher densities and lower temperatures, "closer" to the magnetopause if we use bulk plasma parameters as a proxy for this distance. The location of this nexus between the two branches may be what determined the characteristics of the LPSL in each case. It seems reasonable, for example, that closer to the magnetopause the processes involved in forming the plasma sheet boundary layer would be less important than they might be closer to local midnight, which is consistent with fewer instances of counterstreaming ion beams in the LPSL on March 28. Similarly, the presence of conic-like components in this layer on this date might be associated with low-altitude sources that are stronger away from midnight. In surveys of ion conics during periods of relatively weaker magnetic activity, *Gorney et al.* [1981] and *Kondo et al.* [1990] have shown that their occurrence rates are low near local midnight.

Without composition data we cannot be sure of the sources for the conic-like components observed on March 28; regardless of their origin, if they pass through perpendicular heating regions and then move quasi-adiabatically down the tail, they will have similar appearances. The fact that only the lower-energy components have the kidney shapes suggests that these have histories which are different from those of the higher-energy components. It may be relevant that for the March 28 occurrence the LPSL occurred in association with southward and dawnward IMF directions, when Wind was below the magnetic equator on the dawn side. This is consistent with the results of a survey by *Gosling et al.* [1985], which showed statistically higher densities for the "lobe" in this quadrant and in the dusk, northern quadrant for southward, dawnward IMF orientations. Similarly, higher densities were seen in the adjacent quadrants when the IMF was pointed southward and duskward. For the April 18 case, however, a southward and dawnward IMF orientation was observed prior the appearance of the LPSL, but most of the layer was observed after the IMF had rotated northward; even after accounting for propagation time from IMP 8 to the magnetosphere, there was a lag of ~50 min from the time of southward turning before Wind's first contact with this layer.

One possible approach to identifying the sources of observed particles is the application of multifluid global simulations which can separately track ionospheric and solar wind electron and ion populations [*Winglee*, 1998]. *Li et al.* [2000] employed this approach to demonstrate, among other things, that the hot ion plasma observed by Wind in the magnetotail is mainly of ionospheric origin, and that the heating of this is strongest near the noon-midnight meridian. We note also that the presumed low-altitude source and perpendicular heating mechanism used to explain the kidney-shaped distributions is not the only scenario which might be considered. Near a pinched tail configuration it may be possible to obtain ion distributions which have maxima at pitch angles intermediate between 0° and 90° as the result of nonadiabatic gyrations in the presence of a cross-tail electric field [*Martin*, 1986a, b; *Martin and Speiser*, 1988]. For this explanation to suit, the tail pinch would have to be located interior to Wind's location at 15 R_E on March 28, 1996.

In this paper we have not fully addressed the connection that might exist between the detection of the LPSL and external conditions, such as the orientation of the IMF, solar wind plasma variations, or the state of the magnetosphere.

While the March 28 event appears to be very well correlated with the southward and dawnward turning of the IMF, the ~50 min lag on April 18 between the IMF rotation and the encounter with the LPSL makes such an association unclear. Magnetograms (not shown) from Kiruna, which was near local midnight when Wind encountered the LPSL on April 18, show auroral expansion phase and onset signatures during this interval. On March 28, ground magnetometer data from Fort Churchill show that similar magnetospheric activity was present during this LPSL encounter as well. In a follow-up paper we will examine these and similar questions in more detail, drawing upon additional LPSL encounters, and using POLAR/Ultraviolet Imager observations where possible.

Acknowledgments. We thank Ron Lepping for making the Wind/MFI data available, and A. Szabo for providing the IMP 8 data. We also thank Li-Jen Chen for her contributions of Wind analysis software and her assistance with its use, and Matt Fillingham for providing field line tracing using the Tsyganenko T96 field line model. This research was funded by NASA grants NAG5-4681 and NAG5-8089, and NSF grant ATM-9731951. Hiroshi Matsumoto thanks K. Takahashi and another referee for their assistance in evaluating this paper.

References

Baumjohann, W., Ion and electron heating in the near-Earth tail, in *New Perspectives on the Earth's Magnetotail*, edited by A. Nishida, D. N. Baker, and S. W. H. Cowley, no. 105 in Geophysical Monograph Series, pp. 97–102, American Geophysical Uhion, American Geophysical Uhion, Washington, D. C., 1998.

Eastman, T. E., and E. W. Hones, Jr., Characteristics of the magnetospheric boundary layer and magnetopause layer as observed by Imp 6, *J. Geophys. Res.*, , *84*, 2019–28, 1979.

Eastman, T. E., E. W. Hones, Jr., S. J. Bame, and J. R. Asbridge, The magnetospheric boundary layer: Site of plasma, momentum and energy transfer from the magnetosheath into the magnetosphere, *Geophys. Res. Lett.*, , *3*, 685, 1976.

Eastman, T. E., L. Frank, W. Peterson, and W. Lennartsson, The plasma sheet boundary layer, *J. Geophys. Res.*, , *89*, 1553, 1984.

Eastman, T. E., L. A. Frank, and C. Y. Huang, The boundary layers as the primary transport regions of the Earth's magnetotail, *J. Geophys. Res.*, , *90*, 9541–60, 1985.

Fujimoto, M., T. Mukai, H. Kawano, M. Nakamura, A. Nishida, Y. Saito, T. Yamamoto, and S. Kokubun, Structure of the low-latitude boundary layer: a case study with geotail data, *J. Geophys. Res.*, , *103*, 2297–2308, 1998a.

Fujimoto, M., T. Terasawa, T. Mukai, Y. Saito, T. Yamamoto, and S. Kokubun, Plasma entry from the flanks of the near-Earth magnetotail: Geotail observations, *J. Geophys. Res.*, , *103*, 4391–4408, 1998b.

Fuselier, S. A., B. J. Anderson, and T. G. Onsager, Particle signatures of magnetic topology at the magnetopause: AMPTE/CCE observations, *J. Geophys. Res.*, , *100*, 11,805–11,821, 1995.

Fuselier, S. A., B. J. Anderson, and T. G. Onsager, Electron and ion signatures of field line topology at the low-shear magnetopause, *J. Geophys. Res.*, , *102*, 4847, 1997.

Gorney, D. J., A. Clarke, D. Croley, J. Fennell, J. Luhmann, and P. Mizera, The distribution of ion beams and conics below 8000 km, *J. Geophys. Res.*, , *86*, 83–89, 1981.

Gosling, J. T., D. N. Baker, S. J. Bame, W. C. Feldman, R. D. Zwickl, and E. J. Smith, North-south and dawn-dusk plasma asymmetries in the distant tail lobes: ISEE 3, *J. Geophys. Res.*, , *90*, 6354–60, 1985.

Hall, D. S., M. A. Hapgood, and D. A. Bryant, The transition from the magnetosheath to the magnetosphere, *Geophys. Res. Lett.*, , *17*, 2039–2042, 1990.

Hapgood, M. A., and D. A. Bryant, Re-ordered electron data in the low-latitude boundary layer, *Geophys. Res. Lett.*, , *17*, 2043–2046, 1990.

Horwitz, J. L., C. R. Baugher, C. R. Chappell, E. G. Shelley, and D. T. Young, Conical pitch angle distributions of very low-energy ion fluxes observed by ISEE 1, *J. Geophys. Res.*, , *87*, 2311–20, 1982.

Kondo, T., B. A. Whalen, A. W. Yau, and W. K. Peterson, Statistical analysis of upflowing ion beam and conic distributions at DE 1 altitudes, *J. Geophys. Res.*, , *95*, 12,091–12,102, 1990.

Lepping, R. P., et al., The Wind magnetic field investigation., *Space Sci. Rev.*, *71*, 207–29, 1995.

Li, Q., R. M. Winglee, M. Wilber, L.-J. Chen, and G. K. Parks, The geopause in relation to the plasma sheet and the low latitude boundary layer: Comparison between Wind observations and multi-fluid simulations, *J. Geophys. Res.*, , *105*, 2563–2587, 2000.

Lin, R. P., et al., A three-dimensional plasma and energetic particle investigation for the Wind spacecraft, *Space Sci. Rev.*, *71*, 125–53, 1995.

Lotko, W., and B. U. Ö. Sonnerup, The low-latitude boundary layer on closed field lines, in *Physics of the Magnetopause*, edited by P. Song, B. U. Ö. Sonnerup, and M. F. Thomsen, no. 90 in Geophysical Monograph Series, pp. 371–383, 2000 Florida Avenue, N.W., Washington, DC 20009, 1995.

Lundin, R., Observational and theoretical aspects of processes other than merging and diffusion governing plasma transport across the magnetopause, *Space Science Review*, *80*, 269–304, 1997.

Martin, R. F., Jr., Chaotic particle near a two dimensional magnetic neutral point with application to the geomagnetic tail, *J. Geophys. Res.*, , *91*, 11,985, 1986a.

Martin, R. F., Jr., The effect of plasma sheet thickness on ion acceleration near a magnetic neutral line, in *Ion Acceleration in the Magnetosphere and Ionosphere*, edited by T. S. Chang, no. 38 in Geophysical Monograph Series, American Geophysical Uhion, American Geophysical Uhion, Washington, D. C., 1986b.

Martin, R. F., Jr., and T. W. Speiser, A predicted energetic ion signature of a neutral line in the geomagnetic tail, *J. Geophys. Res.*, , *93*, 11,521, 1988.

Miyake, W., T. Mukai, and N. Kaya, On the evolution of ion conics along the field line from exos d observations, *J. Geophys. Res.*, , *98*, 11,127–34, 1993.

Parks, G., C. Gurgiolo, C. S. Lin, K. A. Anderson, R. P. Lin, F. Martel, and H. Rème, New observations of ion beams in the plasma sheet boundary layer, *Space Sci. Rev.*, *22*, 765–776, 1978.

Parks, G. K., L.-J. Chen, M. McCarthy, D. Larson, R. P. Lin, T. Phan, H. Reme, and T. Sanderson, New observations of ion beams in the plasma sheet boundary layer, *Geophys. Res. Lett.*, *25*, 3285–3288, 1998.

Parks, G. K., et al., Particle and field characteristics of the high-latitude plasma sheet boundary layer, *J. Geophys. Res.*, , *89*, 8885–8906, 1984.

Paschmann, G., W. Baumjohann, N. Sckopke, T. D. Phan, and H. Luhr, Structure of the dayside magnetopause for low magnetic shear., *J. Geophys. Res.*, , *98*, 13,409–22, 1993.

Phan, T. D., and G. Paschmann, Low-latitude dayside magnetopause and boundary layer for high magnetic shear. 1. structure and motion., *J. Geophys. Res.*, , *101*, 7801–15, 1996.

Phan, T. D., et al., The subsolar magnetosheath and magnetopause for high solar wind ram pressure: Wind observations., *Geophys. Res. Lett.*, , *23*, 1279–82, 1996.

Phan, T. D., et al., Low-latitude dusk flank magnetosheath, magnetopause, and boundary layer for low magnetic shear: Wind observations, *J. Geophys. Res.*, , *102*, 19,883–19,895, 1997.

Scholer, M., and R. A. Treumann, The low-latitude boundary layer

at the flanks of the magnetopause, *Space Sci. Rev.*, *80*, 341–367, 1997.

Sharp, R. D., D. L. Carr, W. K. Peterson, and E. G. Shelley, Ion streams in the magnetotail, *J. Geophys. Res.*, , *86*, 4639–4648, 1981.

Song, P., B. U. Ö. Sonnerup, and M. F. Thomsen (Eds.), *Physics of the Magnetopause*, no. 90 in Geophysical Monograph Series, American Geophysical Union, 2000 Florida Avenue, N.W., Washington, DC 20009, 1995.

Song, P., et al., Structure and properties of the subsolar magnetopause for northward interplanetary magnetic field; multiple-instrument particle observations., *J. Geophys. Res.*, , *98*, 11,319–37, 1993.

Takahashi, K., and E. W. Hones, Jr., ISEE 1 and 2 observations of ion distributions at the plasma sheet-tail lobe boundary, *J. Geophys. Res.*, , *93*, 8558–8582, 1988.

Tsyganenko, N. A., A magnetospheric magnetic field model with a warped tail current sheet, *Planetary and Space Science*, *37*, 5–20, 1989.

Tsyganenko, N. A., and D. P. Stern, Modeling the global magnetic field of the large-scale birkeland current systems, *J. Geophys. Res.*, , *101*, 27,187–27,198, 1996.

Whalen, B. A., S. Watanabe, and A. W. Yau, Observations in the transverse ion energization region, *Geophys. Res. Lett.*, , *18*, 725–728, 1991.

Winglee, R. M., Multi-fluid simulations of the magnetosphere: the identification of the geopause and its variation with IMF, *Geophys. Res. Lett.*, , *25*, 4441–4444, 1998.

Q. Li, M. McCarthy, R. M. Winglee, University of Washington, Geophysics, ATG Building, Box 351650, Room 202, Seattle, WA 98195-1650, winglee@geophys.washington.edu, mccarthy@geophys.washington.edu).

R. P. Lin, G. K. Parks, M. Wilber, University of Cailifornia at Berkeley, Space Sciences Laboratory, Rm. 360, Centennial Dr. at Grizzly Peak Blvd., Berkeley, CA 94620, parks@ssl.berkeley.edu, boblin@ ssl.berkeley.edu).

(Received June 15, 2000; revised September 19, 2000; accepted November 6, 2000.)